Original Research Article

J. Funct. Mater. Biomol. 1(2)-2017 pp 76-86

SACRED HEART RESEARCH PUBLICATIONS

Journal of Functional Materials and Biomolecules

Journal homepage: www.shcpub.edu.in

ISSN: 2456-9429

Investigation on the properties of formamidinium tin strontium iodide systems

Lucangelo Dimesso*

Received on 24 Oct 2017, Accepted on 9 Dec 2017

Abstract

The properties of formamidinium-tin-strontium iodide systems as promising candidate for optoelectronic applications were investigated. Orthorhombic FASnI3 (space group *Amm2*) and SnI_2 were detected as major crystalline phases. Static thermogravimetric analysis under nitrogen revealed a decrease of the weight loss rate at increasing the Sr-content. The optical spectra displayed a decrease of the absorption edges (1015nm, x = 0.0, 950-960nm, x = 0.1) and revealed a direct semiconducting behavior with band energy gaps of 1.31eV-1.34eV. The photoluminescence profiles (excitation wavelength λ_{exc}=380nm) showed large emission bands at ~845nm, ~920nm, ~969nm) and for λ_{exc} = 500nm at ~681nm, ~1063nm and ~1085nm respectively.

Keywords: Hybrid perovskites, optoelectronic, formamidinium tin iodide.

1 Introduction

Organic–inorganic hybrid halide perovskites have in the past few years attracted intense attention as the most promising materials for light-emitting diodes, lasers, photo-detectors [1] and solar cells with power conversion efficiency (PCE) over 22% [2 and references in there]. Organic-inorganic perovskites are crystalline materials with a typical ABX_3 structure where the A cation resides at the eight corners of a cubic unit while the B cation is located at the center of octahedral $[BX_6]^{4-}$ structure. In the most common organic-inorganic halide perovskites, the A position represents an organic or metal cation, e.g., $CH_3NH_3^+$ (methylammonium MA), $HC(NH_2)_2^+$ (formamidinium, FOR) and/or Cs^+, B a divalent metal cation (typically Pb, Sn, Ge) and X an halide (I, Br and/or Cl). Along with the advantages of cost-effective solution-process, the fabrication of solar cells is now comparable to state-of-the-art commercial photovoltaic techniques including silicon, CdTe, CuInGaSe, and GaAs, fulfilling the requirements for the large-scale deployment of solar energy. Moreover, organic-inorganic hybrid perovskites such as the archetype methylammonium lead iodide ($MAPbI_3$) are obtained from abundant chemical precursors [3, 4]. Unfortunately, the toxicity issue of lead (Pb) has led to a bottleneck to further development. The maximum Pb^{2+} content was set at the level of 0.15 μg L^{-1} and 15 μg L^{-1} in air and water, respectively, by the U.S. EPA [5] and 0.5μg / m^3 in air, ≤ 5.0μg / L in drinking water respectively by the European Commission on Health and Environment Risks [6, 7]. PbI_2 is the product of the decomposition of perovskites and has a larger solubility (K_{sol} on the order of $1x10^{-8}$) than the conventionally toxic Cd^{2+} in CdTe (K_{sp} on the order of 1 $x10^{-22}$) [8] which have been processed with recycling progress in past years due to its toxicity. This indicates a higher toxic level of Pb^{2+} than Cd^{2+} in their corresponding solar cells materials. Toxicity, long degradation lifetime, and stability in the ecosystem determine a very long time pollution of the soil or water. The facts also imply that the pollution of lead in our living earth will be hard to control if mass production of conventional $MAPbI_3$ solar cells is realized [9]. As a similar element to Pb, tin (Sn) has been reported to be an alternative in lead-free perovskites. Pb and Sn have similar ionic radii (six-fold coordination, high spin, Pb^{2+}: 1.19 Å [10]; Sn^{2+}: 1.18Å [11]) and this might encourage Sn to substitute Pb with no significant perturbation in lattice structure. Besides, Sn-based perovskites have a narrower optical band gap of and a higher charge mobility of $\approx 10^2$–10^3 $cm^2/V{\cdot}s$ (Pb-based perovskite ≈10–10^2 $cm^2/V{\cdot}s$) [12]. These promising photovoltaic properties can be partly due to inactive Sn(II) outer shell orbitals, like inactive Pb *6s* orbital in the perovskite structure. However, Sn^{2+} is relatively unstable and easily oxidized to Sn^{4+} leading to self-doping due to a *p*-type Sn^{4+} act. In addition, upon moderate exposure to external stimuli (such as humidity, oxygen, elevated temperature or a combination of these factors) these perovskites tend to degrade into harmful compounds carrying heavy metals, which may readily leach into the environment as a result of the structural failure of a photovoltaic module [13-15]. According to International Standards (IEC 61646 climatic chamber tests), long-term stability at 85°C (representing an elevated temperature on a roof on a hot summer day) is required in order to compete with the silicon-based technology [15]; furthermore the material should be stable till 150°C a typical curing temperature for ethylene-vinyl acetate and many other commercial encapsulants.

Recently we investigated the thermal stability of Sn^{2+} containing $CH_3NH_3Sn_xI_3$ powder systems (with $0.9 \leq x \leq 1.1$) by static thermogravimetry in inert (nitrogen) and

* Corresponding author e-mail: ldimesso@surface.tu-darmstadt.de,
Phone: +0049-6151-16 20779, Fax: +0049-6151-16 20771
Technische Universität Darmstadt, Material and Geosciences Department
Otto-Berndt-Strasse 3, D-64287 Darmstadt, Germany

oxidizing atmospheres (air) [16]. The samples measured at constant temperature (T= 85°C and T =150°C respectively for t= 2 h) recorded a linear weight loss as a function of the time. Supported by the elemental analysis, the weight loss was associated to iodine (-containing) species which confirmed previous assessments [17]. In order to improve the thermal stability of the Sn-based perovskites and to counteract the acidification that follows from HI formation during perovskite degradation, a further step of our investigation was the addition of earth-alkaline ions (i.e. Mg, Ca, Sr) into the starting composition of the Sn-containing perovskites [18]. We found out that the addition of earth-alkaline ions led to an improvement of the thermal stability of the Sn-containing perovskites at 85°C under nitrogen as well as to an increase of the photoluminescence intensity. These results encouraged us to extend the investigation to the formamidinium containing Sn-perovskites. Purpose of this work is the investigation of structural, microstructural, optical, photoluminescence (PL) properties of strontium containing Sn-based hybrid perovskites systems (For SI, $CH(NH_2)_2Sn_{1-x}Sr_xI_3$ ($0.0 \leq x \leq 0.1$)). Results on the thermal stability of the systems in nitrogen are also discussed.

2 Experimental

Formamidinium tin iodide powders containing Sr-ions ($CH(NH_2)_2Sn1_{-x}Sr_xI_3$ ($0.0 \leq x \leq 0.1$) were prepared by a precipitation process in aqueous solutions obtained by commercially available materials. In particular, $Sn(CH_3COO)_2$ (tin(II) acetate, Alfa Aesar), HI (47% wt., hydroiodic acid stabilized with 1.5% wt hypophosphorous acid, Alfa Aesar), $HN{=}CHNH_2{\bullet}CH_3COOH$ ($C_3H_8N_2O_2$, formamidine acetate, Sigma Aldrich), $SrCO_3$ (strontium carbonate, Aldrich) were used as delivered. The materials were prepared by addition of a corresponding amount of $C_3H_8N_2O_2$ at T = 110°C in aqueous solutions containing Sn^{2+} and Sr^{2+} ions (For : Sn (+ Sr) = 1 : 1 molar ratio) in air. In order to avoid the Sn(II) oxidation into Sn(IV), 3.5mL H_3PO_2 solution (hypophosphorous acid, 50% wt., Fischer Scientific, UK) was added into starting solution (9.0mL) during the heating step up to 110°C [18-20]. After cooling down the solution to room temperature, the prepared black powders were separated from the mother liquor and rinsed with distillate water and 2-propanol. In order to avoid any surface contamination or reaction we stored the samples in a glove-box under Ar-atmosphere (≤ 5 ppm H_2O).

Thermal, structural, microstructural analyses, optical diffuse-reflectance measurements and the estimation of the band gap of the materials were carried out as reported in our previous work [18]. The photoluminescence (PL) measurements were performed by a VARIAN Cary Ellipse fluorescence spectrophotometer equipped with a Xe-arc as emission source. The emission was measured in the 650-1100 nm range. All measurements were performed at room temperature.

3 Results and Discussion

The thermal properties of the as prepared $CH(NH_2)_2Sn_{1-x}Sr_xI_3$ systems were investigated by dynamic differential thermal analysis (DTA) and dynamic thermogravimetry (TG) in the range between 30°C to 600°C (heating rate of 10K/min) under flowing nitrogen and air. As example, DTA and TG curves (and their derivatives for a better resolution of the thermal profile) of the $CH(NH_2)_2Sn_{1-x}Sr_xI_3$ system (For SI, x=0.0), under nitrogen, are shown in Figure 1A and Figure 1B respectively. The peaks of the thermal events, from the derivative curves, are summarized in Table 1.

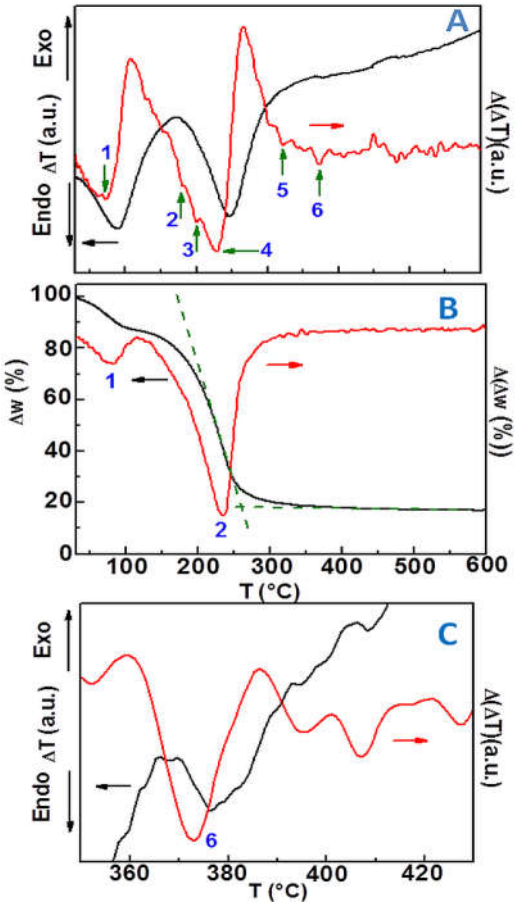

Figure 1 Typical A) Dynamic DTA and B) TG profiles (with the corresponding first derivative curves, 10 K/min) of the $HC(NH_2)_2Sn_{1-x}Sr_xI_3$ system performed under flowing nitrogen (in this case x = 0.0); C) enlargement of the thermal profile in Figure 1A. The peak temperatures are reported in Table 1.

The evaluation of the first derivative curves of the DTA profiles (Figure 1A) showed major endothermic events (labeled with "2", "3" and "4", Table 1) peaking at T= 178°C, T=200°C and T=228°C respectively. Additional thermal events were detected at T=72°C (labeled with "1"), T= 320°C and T=373°C (labeled as "5" and "6") respectively. The thermal peak at T=72°C can be related to the evaporation of rinse solvents as confirmed by the thermogravimetric profile (Figure 1B) and the thermal event "5" can correspond to the melting process of solid

Sn(II) iodide (melting point at T = 320°C [21]) which is a by-product of the decomposition of Sn-containing perovskites. On the other hand, the thermal events "2", "3" and "4" were attributed to decomposition processes of the ForSI system as confirmed by the weight losses recorded in the thermogravimetric profile (Figure 1B, Table 1).

Table 1 Values of the thermal events for the ForSI (x = 0.0) system obtained from the derivative curves in Figure 1A and in Figure 1B respectively.

	Therm. event nr.	T_p (°C)	Endo/Exo
DTA	1	72	Endo
	2	178	Endo
	3	200	Endo
	4	228	Endo
	5	320	Endo
	6	373	Endo
TG	1	80	
	2	229	

Unlike the decomposition of $CH_3NH_3SnI_3$ (*s*) which can lead to the formation of methylamine and SnI_2 [22] or to CH_3I and NH_3 as recently reported [18 and references in there], the decomposition process of formamidine can give rise to the formation of ammoniac and hydrogen cyanide according to the reaction

$$HC(NH_2)NH \rightarrow NH_3 + HCN \quad (1a)$$

Indeed "*ab initio*" studies [23, 24] using Gaussian-*n* theories predict the reaction to be exergonic both in gas phase and in solution, where formation of the separated species (HCN + NH_3) is favored over formation of the complex (HCN–NH_3) due to the increase of entropy for the formation of separated products, which means that the overall decomposition of ForSI can occur as follows

$$HC(NH_2)NH_2SnI_3\ (s) \rightarrow HCN\ (g) + NH_3\ (g)\ HI\ (g) + SnI_2\ (s) \quad (1b)$$

followed by the melt reaction

$$SnI_2\ (s) \rightarrow SnI_2\ (liq) \quad (2)$$

The processes 1(b) and (2) can be confirmed by the broad DTA-event (Figure 1A) as well as by the absence of a "plateau" in the TG-curve (Figure 1B). Furthermore, the thermal event "6" in Figure 1A can be related by the disproportion of SnI_2 (*liq*) into liquid metal Sn (0) and SnI_4 vapors according to the reaction

$$SnI_2\ (liq) \rightarrow Sn\ (s) + SnI_4\ (g) \quad (3)$$

This fact is supported by the thermal data: (i) the thermal peak lies at T ≈ 373°C (as shown in the enlargement of the DTA profile in Figure 1C) which is very close to the boiling point of SnI_4 (T = 364.35°C [21]) and (ii) the TG-profile revealed, at T ≈ 373°C, a residual of ≈ 21.0 wt% (Figure 1B) which is very close to the theoretical value of 21.8 wt% according to the reactions (1) to (3) (Figure S1 in Supplementary Information).

In order to better understand the influence of the thermal treatments on the structural and microstructural properties of the ForSI system, annealing under nitrogen atmosphere were carried for t = 8 hr in a range of temperature between 115°C and 230°C. The XRD patterns for the as prepared FASnI3 (ForSI), used as comparison, and after the thermal treatments are shown in Figure 2. Unlike the analogous Pb-containing compound $FAPbI_3$ possessing two polymorphs (black and yellow) in which the presence of the non-perovskite yellow polymorph restricts the photovoltaic performance of the solar cells [12, 25], the XRD peaks of the as prepared ForSI sample (Figure 2A) and after annealing at different temperatures (115°C, Figure 2B and 150°C, Figure 2C) indicate that the orthorhombic FASnI3 phase (space group *Amm2* [12]) exists over this temperature range [26, 27].

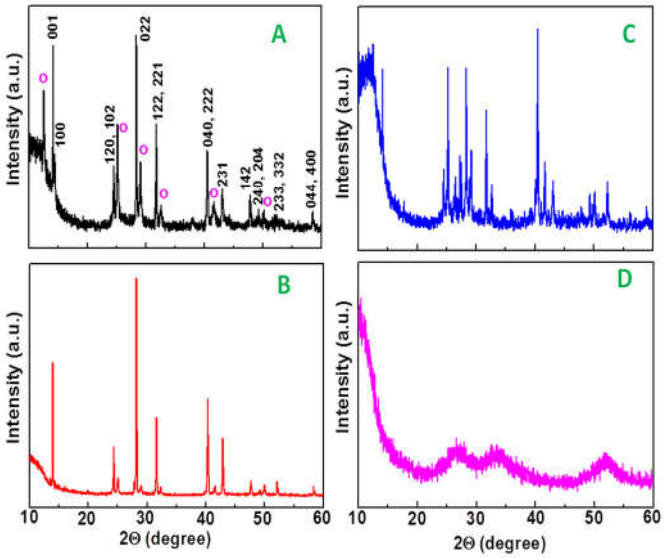

Figure 2 Typical XRD patterns of $HC(NH_2)_2SnI_3$ system (x = 0.0) A) as-prepared and after thermal treatment for t = 8 hr under nitrogen at B) T = 115°C, C) T = 150°C and D) T = 230°C respectively. "o" indicates the monoclinic SnI_2 phase.

Moreover, crystalline reflections attributed to monocline SnI_2 (labeled with "o" in Figure 2A) and further crystalline reflections of not identified phase(s) (Figure 2C) were detected. After annealing at T = 230°C the XRD pattern showed the presence of broad halos (Figure 2D) which indicate the formation of non-crystalline phases possibly due to a degradation process of the ForSI crystallites. This process was observed during our investigations on methylammonium tin iodide, after annealing in air at T= 150°C [16] and explained by supposing a reaction of the oxygen atoms with the Sn-ions of the perovskite through defects, dislocations in the crystalline structure of the $MASnI_3$ phase. The amorphization of Sn-containing perovskite (under argon)

has been recently reported by Lü [28] by compressing the prepared powders till 31.2GPa using a diamond anvil at room temperature (no information on investigations as a function of the temperature are reported in the published work). The authors observed a transformation from crystalline into amorphous state and a return to the crystalline state after decompression to ambient pressure. However in our case, under nitrogen, the formation of non-crystalline phase is associated with weight losses occurring at the annealing temperature which clearly indicate an irreversible decomposition process.

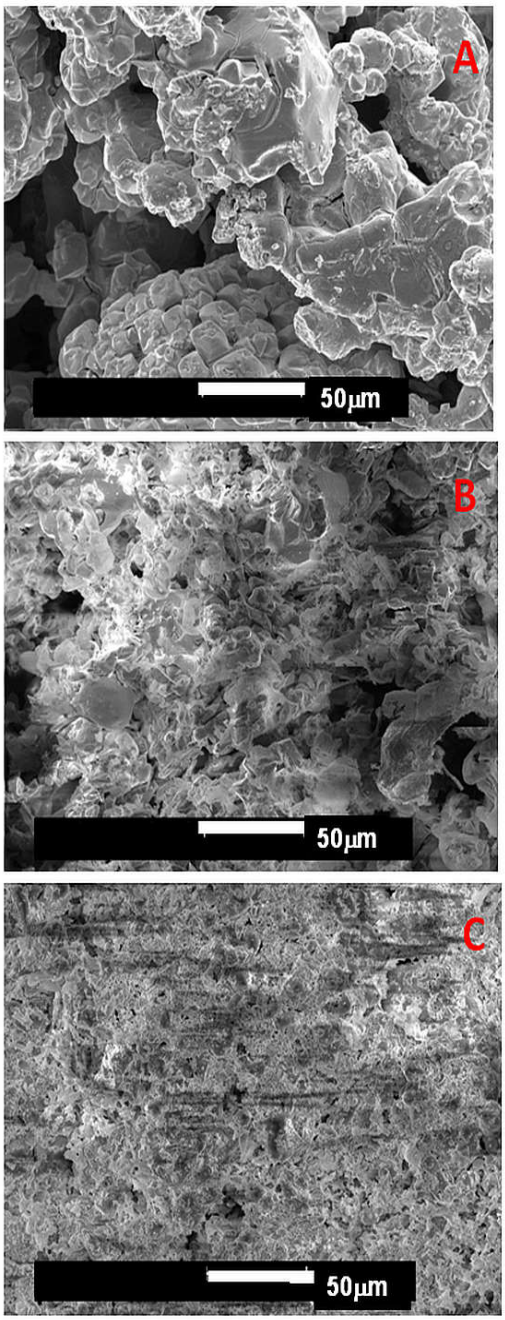

Figure 3 SEM-images of $HC(NH_2)_2SnI_3$ system (x = 0.0) A) as prepared and after annealing (t = 8 hr) under nitrogen at B) T = 150°C and C) T = 230°C respectively.

The morphological analysis, performed on the as-prepared sample and after annealing (t = 8 hr) under nitrogen at T = 150°C and T = 230°C (shown in Figure 3A, Figure 3B and Figure 3C) revealed the formation of irregularly shaped crystallites with flat surface due to the crystallization conditions of the sample (Figure 3A); on the other hand after the annealing at T = 150°C the formation of a not identified crystalline phase (as white layer in Figure 3B) was observed. This layer could indicate the growth of an "intermediate" phase before a process of degradation of the crystallites takes place and further continue as shown in Figure 3C.

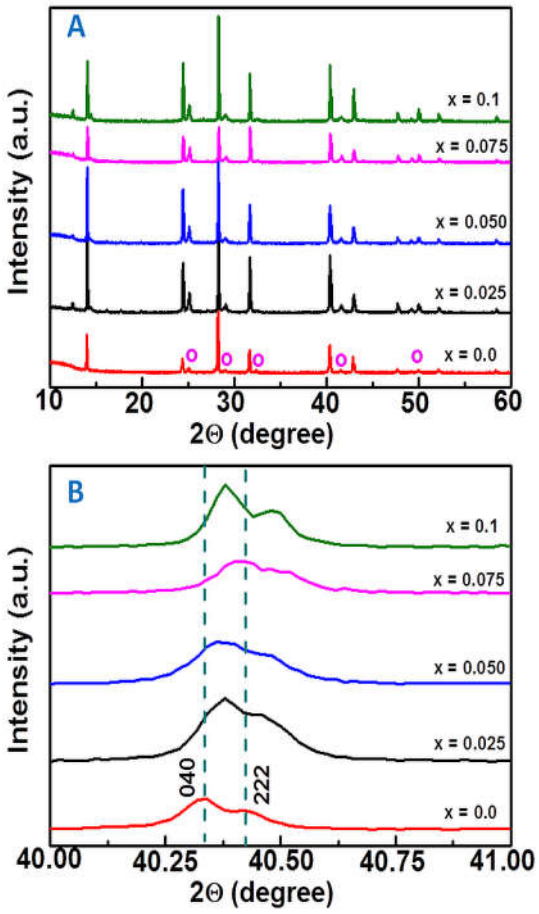

Figure 4 A) XRD patterns of the $HC(NH_2)_2Sn_{1-x}Sr_xI_3$ systems ($0.0 \leq x \leq 0.1$) after annealing at T = 115°C (t = 8hr) under nitrogen; B) enlargement of Figure 4A. "o" indicates the monoclinic SnI_2 phase.

The effects of the addition of Sr-ions on the structural properties of the $CH(NH_2)_2Sn1_{-x}Sr_xI_3$ phase ($0.0 \leq x \leq 0.1$) are shown in the XRD patterns in Figure 4A and in the enlargement in Figure 4B respectively. By observing the XRD diffractogramms, there are some important points to note. First, the pattern for the Sr-containing ForSI phase showed diffraction peaks, which can be indexed to planes of the orthorhombic *Amm2* space group [12, 25-27] and reveal the presence of crystalline reflections (indicated with "o" in Figure 4A) assigned to monoclinic SnI_2 (pattern 01-070-1492 in ICSD database). In the Pb-containing analogous, compared to $CH_3NH_3^+$, $HC(NH_2)_2^+$ possesses higher temperature stability as was highlighted in the

black polymorph of $HC(NH_2)_2PbI_3$ [26]. The higher stability of the $HC(NH_2)_2^+$ analogue could arise due to a more rigid perovskite structure from the enhanced hydrogen bonding between $HC(NH_2)_2^+$ cations and the inorganic matrix [29]. Furthermore, this halide does not undergo any phase transitions up to a temperature of 150°C, indicating that this perovskite would be a much more stable alternative than the commonly explored methylammonium containing perovskites. Second, the enlarged patterns (Figure 4B) revealed a shift of the positions of (040) and (222) crystalline reflections towards higher diffraction angles in the Sr-containing systems. The shift increases at increasing the Sr-content till x = 0.075 and can be explained by the incorporation of the Sr^{2+}-ions into the perovskite structure and can be related to variations in lattice parameters and unit cell volume of the ForSi phase which can be understood on the basis of the different the different properties (polarity, coordination number) between Sn^{2+}- and Sr^{2+}-ions being the ionic radii very similar (six-fold coordination, high spin, Sn^{2+}: 1.18Å and Sr^{2+}: 1.18Å respectively [10]). The microstructural analysis revealed the formation of coarse powder in the Sr-containing systems but no dramatic changes in the morphology as shown in Figure S2A and Figure S2B respectively.

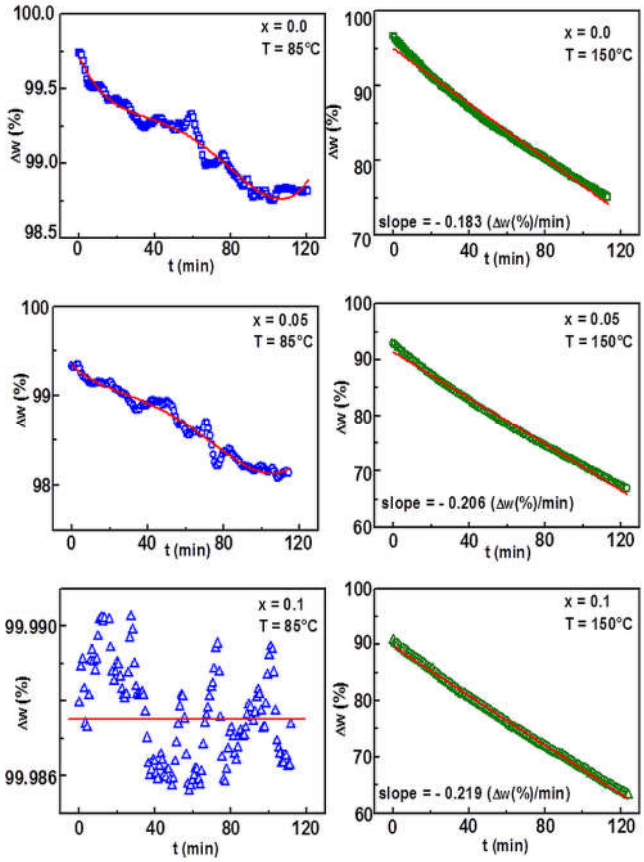

Figure 5 Isothermal curves of the $HC(NH_2)_2Sn_{1-x}Sr_xI_3$ systems recorded at T = 85°C and T = 150°C (t = 2h under nitrogen) for x = 0.0, x = 0.05 and x = 0.1 respectively. The solid red lines are the fit of the data originated by the program OriginPro 8. The corresponding fit parameters are reported in Table S1.

The effects of Sr-ions addition on the thermal stability of the For-Sn-Sr-I systems were investigated by static TG-analysis in nitrogen. The samples have been heated up to T = 85°C and to T = 150°C respectively and weight losses were measured in a time range t = 2h. The weight losses of $(CH(NH_2)_2Sn1_{-x}Sr_xI_3$ (for x = 0.0, 0.05 and 0.1) as a function of time at constant temperature in nitrogen are shown in Figure 5. The loss rates (wt% / minute) were calculated by fitting the experimental data; the corresponding fit parameters are summarized in Table S1. At T = 85°C, the ForSI system (x = 0.0) the estimated weight loss showed is exponentially dependent upon the time (-0.0268 wt%/min in the linear approximation by neglecting the contribution of higher orders as in Figure 5). Indeed the data were fit by a polynomial relationship of order 4 with asymptotic behavior till t ≈ 100 min then no further loss was recorded. Although the weight loss rate of ForSI is higher than the methylammonium tin iodide phase (-0.0039 wt%/min [16]) the obtained thermal data confirmed the higher thermal stability of the formamidinium containing tin organic-inorganic perovskite compared to methylammonium tin iodide which showed a linear dependence of the weight loss as a function of the time in the same investigated range of time. The addition of Sr-ions showed an enhancement of the thermal stability of the $CH(NH_2)_2Sn_{1-x}Sr_xI_3$ phase; for x = 0.05 an estimated weight loss of -0.0197 wt%/min was obtained by the linear approximation of the polynomial fit of the data (Table S1) whereas for x = 0.1 a barely measurable weight loss was recorded (Table S1). This behavior can be explained by the very similar ionic radii of Sn(II) and Sr(II) which can be exchanged in the central position of the perowskite $[MI_6]^{4-}$octahedra; furthermore, the stronger polarization of the Sr-I bonds may bind iodine anions more tightly and consequently may reduce the formation of volatile iodine (-containing) species. On the other hand, the static TG measurements performed in nitrogen at T = 150°C revealed a linearly dependence of the weight loss as a function of time and higher weight loss rates than those at lower temperature (Table S1). The ForSI system showed a weight loss rate of -0.1835wt%/min whereas an increase of the weight loss rates was recorded (-0.2063 wt%/min for x = 0.05 and -0.2162 wt%/min for x = 0.1 respectively). A possible explanation is the lower stability of Sr-I ionic bonds at higher temperature compared to the Sn-I covalent bonds into the $[SnI_6]^{4-}$ octahedra which favors the decomposition of the perovskite as confirmed by the dynamic thermal profile in Figure S1 (red curve).

The addition of Sr-ions in the For-Sn-I system can have a dramatic influence on the optical properties of the prepared materials. In Figure 6A the absorption spectra of $ForSn_{1-x}Sr_xI_3$ systems ($0.0 \le x \le 0.1$) are shown. Assuming a bulk-like behavior, the adsorption edges ($\lambda_{on\text{-}set}$ (nm), the frequency value at which the photons absorption begins) can be obtained obtained by fitting the linear part of the absorbance spectrum [4, 5]. The values of the adsorption edges are reported in Table 2. By observing the optical spectra in Figure 6 and the data in Table 2 following points are to note. First, the adsorption spectra displayed a strong,

abrupt absorption in infrared region which decreases from 1015nm (x = 0.0) to 950-960nm (as in Table 2) by increasing the Sr-content into the starting composition. The optical absorption value of the ForSI phase is higher than that observed in the Pb-analogue (880nm) [25] and lower than those recently observed in the MA-Sn-Sr-I systems [18]. Nevertheless, the sharp absorption even at lower Sr-content (x < 0.1) would indicate a less important contribution of the secondary phases to the optical profile. Second, the addition of Sr-ions decreases dramatically the higher absorbance background in the optical profiles (Figure 6A). Indeed the high absorbance background is a feature of the Sn-containing hybrid systems [14, 18] and recently we reported that the addition of Sr-ions in the MA-Sn-I systems further increased the threshold of the background. This was explained, supposing strong scattering effects of the Sn^{2+}-ions can act like scattering centers as recently reported by our group [30] during our investigations on the methylammonium tin-strontium iodides. We supposed that the addition of (Sr)-ions (and generally earth-alkaline ions) increased the population of the scattering centers by promoting the formation of second-phase particles such as inclusions and/or precipitates during the crystallite growth and/or the cooling process during the preparation of the materials. In this case, the higher stability of the formamidinium containing system can give origin to a decrease of the optical background.

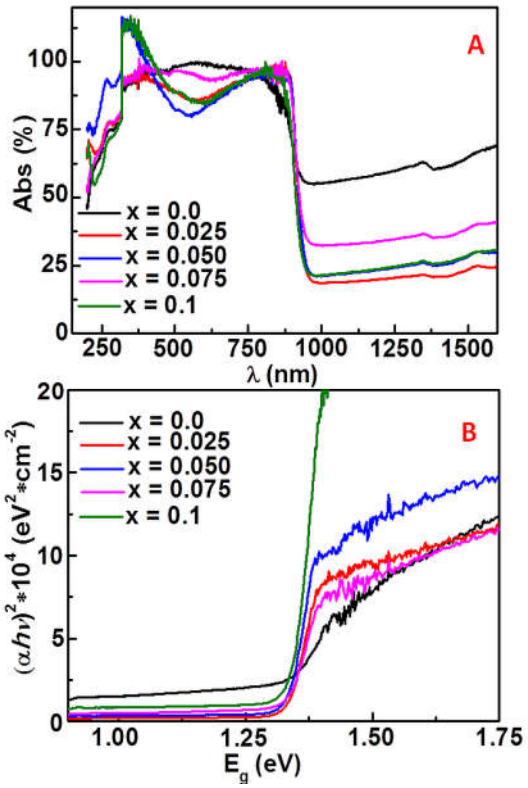

Figure 6 A) Normalized optical absorption spectra and B) plots $(\alpha h\nu)^2$ for direct transitions, where α is absorption coefficient and $h\nu$ is photon energy, of $HC(NH_2)_2Sn_{1-x}Sr_xI_3$ systems ($0.0 \le x \le 0.1$). The values of the band gap energy (E_g), obtained by extrapolation to α=0, are reported in Table 2.

As nano-particle powders tend to agglomerate and consequently to develop bulk-like bands, the relationship between the adsorption coefficient (α) near the absorption edge and the optical band gap (E_g) for direct interband transitions obeys a relationship as previously reported [4, 16].The plots derived from the relationship, leads to graphics as shown in Figure 6B. By extrapolating to α = 0, the plots revealed a behavior of a direct semiconductor with band energy gaps between 1.31eV (x = 0.0) and 1.34ev (x = 0.1). The similar values of the band gap energy may be related to the replacement between Sr- and Sn-ions which had low influence on the "nature" of the defects, vacancies and impurities formed during the crystallites growth.

Table 2 Optical and photoluminescence properties of the $HC(NH_2)_2Sn_{1-x}Sr_xI_3$ systems. The adsorption edges ($\lambda_{on\text{-}set}$ (nm)) were obtained by fitting the linear part of the absorbance spectra in Figure 6A according to the model proposed in Ref. [4]. The optical band gap energy values, obtained from the data in Figure 6B were calculated according to the model in Ref. [4].

x	$\lambda_{on\text{-}set}$ (±2nm)	E_g (±0.01eV)
0	1055	1.31
0.025	948	1.33
0.050	948	1.33
0.075	959	1.33
0.100	948	1.34

The photoluminescence (PL) spectra of the $CH(NH_2)_2Sn_{1-x}Sr_xI_3$ phase ($0.0 \le x \le 0.1$), measured at room temperature and excitation wavelengths λ_{exc} = 380 nm and λ_{exc} = 500 nm, are shown in Figure 7A and Figure 7B respectively. The PL-spectrum of the ForSI system (x = 0.0) at λ_{exc} = 380nm an emission band peaking at ~845nm (labeled with "1" in Figure 7A) with a broad shoulder at ~865nm (labeled with "2") were detected in the 700nm – 1100nm range with additional bands peaking at ~920nm ("3" in Figure 7A) and at ~969nm ("4" in Figure 7A) respectively. Similar shapes of PL-spectra were recently reported by Fang [31] during their investigation of nanocrystalline ensembles and polycrystalline layer of the Pb-containing analogue. The authors observed PL-bands peaking at higher wavelengths (~855nm), however the measurements were recorded at low temperatures (25-35 K) where the formamidinium lead iodide adopt an orthorhombic crystalline structure [31 and references in there]; these emissions were attributed to free excitons and bound excitons with singlet and triplet characters, respectively. The addition of Sr-ions affected the emission properties of the ForSI phase. Indeed, an increase of the

PL-band intensity at increasing the Sr-content was observed with a maximum at x = 0.05, then the PL-intensity decreases. The increase of the PL-intensity as a function of the Sr-content was previously observed by our group during the investigation of earth-alkaline containing $MASnI_3$ systems [18] and explained by supposing the incorporation of Sr-ions into the perovskite crystalline structure and their interaction with the iodine ions which change the local field strength of the Sn-ions in the $[SnI_6]^{2-}$ octahedra as observed in oxide phosphors [32-34]. This interaction can cause an increase of the local disorder into the crystalline lattice and the observed effect of this greater disorder is detected by the higher values of the luminescence intensity. At higher Sr-content a quenching effect may take place with a consequent decrease of the PL-intensity [34].

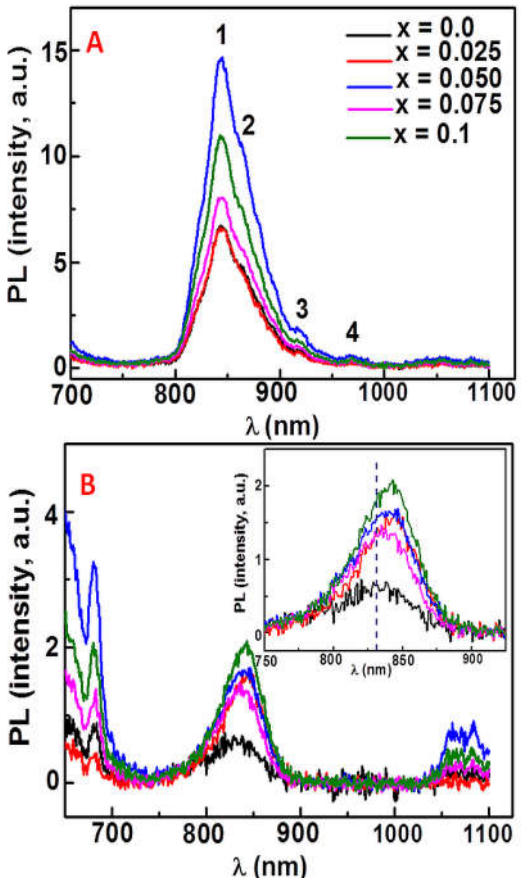

Figure 7 PL-emission spectra of $HC(NH_2)_2Sn_{1-x}Sr_xI_3$ systems ($0.0 \leq x \leq 0.1$) measured (at room temperature) with excitation wavelengths of A) λ_{exc} = 380nm and B) λ_{exc} =500nm respectively. The inset in Figure 7B is an enlargement of the range 750nm-950nm. The y-axis values indicate the PL-intensity ratios compared to the ForSI (x = 0.0) system only.

An increase of the emission peak intensity by adding Sr-ions into the ForSI crystalline structure was observed by increasing the excitation wavelength. The PL-profiles of the $CH(NH_2)_2Sn_{1-x}Sr_xI_3$ phase systems measured at excitation wavelength λ_{exc} = 500nm in a the range 650-1100nm (Figure 7B) revealed emission peaks at ~681nm, broader emissions peaking at ~1063nm and ~1085nm respectively and emission peaks at ~830-840nm; the intensity of the emissions increased by increasing the Sr-content reaching a maximum for x = 0.05. The emission peaks at ~681nm are typical PL-features of iodide containing systems and were also observed during our investigations of Cs-Sn-I [30] and MA-Sn-I systems [16]. Indeed these PL-emissions were detected in SnI_2 doped CdI_2 crystals [35], attributed to electron-hole recombination on halogen vacancies, followed by energy transfer, via an Auger process, to emission centers involving interstitial Cd as well as in Pb^{2+}-doped SrI_2 crystals [36] and connected with different Pb-centers formed in SrI_2, that means, a portion of PbI_2 may segregate in SrI_2 host and result in formation of the unwanted scattered centers. On the other hand, the broad emissions in the range 1030-1100nm were also observed in methylammonium tin iodide perovskite structures and related to Sn-vacancies which are the most favorable intrinsic defect and can act as active scattering centers [12, 16]. Finally unlike the $MASnI_3$ phase, the emission peaks at ≈830-840nm are typical PL features of the formamidinium-containing systems; this emission, peaking at ≈838nm, was observed by Wang [37] during the investigation of pressure-induced structural and electronic changes of the α-$FAPbI_3$ phase. To note in our case that the addition of Sr-ions (i) increases the emission intensity reaching a maximum for x = 0.05, then it decreases; (ii) shifts the emission peaks from ~830nm (x = 0.0) to ~842nm (x = 0.1) as shown in the inset of Figure 7B. This can be explained by the similar ionic radius between Sn^{2+} and Sr^{2+} ions which can be easily exchanged in the $[SnI_6]^{2-}$ octahedra. The exchange changes the local environment of the Sn^{2+} and possibly stabilizes the perovskite structure by changing the mechanism of the spectroscopic transitions and favoring higher intensity of the luminescence emissions without changing the nature of the emission bands.

4 Conclusions

In this work the investigation of structural, microstructural, optical, photoluminescence (PL) properties of $CH(NH_2)_2Sn_{1-x}Sr_xI_3$ (formamidinium tin strontium iodide, $0.0 \leq x \leq 0.1$) prepared by precipitation process in acidic aqueous solutions and annealing in nitrogen is reported.

The derivative profile under nitrogen of the dynamic differential analysis showed major endothermic events peaking (T = 178°C, T = 200°C and T = 228°C respectively) attributed to decomposition processes of the ForSI system as confirmed by the weight losses recorded in the thermogravimetric profile. Additional thermal events (T = 72°C, T = 320°C and T = 373°C respectively) were related to the evaporation of rinse solvents, to the melt process of solid Sn(II) iodide and to the evaporation of SnI_4 vapors as by product of the disproportion of SnI_2 respectively.

The XRD patterns samples revealed the presence of the orthorhombic FASnI3 phase (space group *Amm2*) as major crystalline phase, and monocline SnI_2. Additional crystalline reflections were detected after annealing at T =

150°C and the formation of non-crystalline phases was observed after annealing at T = 230°C as confirmed by the morphological analysis. The addition of Sr-ions shifted the positions of crystalline reflections towards higher diffraction angles; the shift was explained by the incorporation of the Sr^{2+}-ions into the perovskite structure and related to variations in lattice parameters and unit cell volume of the ForSi phase. The static thermogravimetric measurements under nitrogen at T = 85°C revealed a decrease of the weight loss rate at increasing the Sr-content and for x = 0.1 a barely measurable weight loss was recorded. On the other hand, the measurements at T = 150°C revealed an increase of the weight loss rate at increasing the Sr-ions into the composition possibly due to formation of Sr-I ionic bonds which are weaker than the Sn-I covalent bonds.

The optical adsorption spectra displayed a sharp absorption in infrared region which decreases from 1015nm (x = 0.0) to 950-960nm (x = 0.1) and a decrease of the absorbance background in the optical profiles possibly due to a decrease of the population of the scattering centers. The Tauc plots revealed a direct semiconducting behavior with band energy gaps in the range of 1.31eV and 1.34eV. The photoluminescence (PL) spectra (excitation wavelength λ_{exc} = 380nm) showed emission bands at ~845nm, ~920nm and ~969nm respectively whereas at λ_{exc} = 500nm emission peaks at ~681nm, ~1063nm and ~1085nm were detected with additional emission peaks shifting from ~830 nm for x = 0.0 till ~840nm for x = 0.1 and increasing PL-intensity. The increase of the intensity of the photoluminescence response can open new field of application for Sr- containing For-Sn-I perovskites beyond photovoltaic and solar cells.

Acknowledgements

The author is grateful to Prof. W. Jaegermann and to Dr. T. Mayer for giving him the support in this work and for the valuable discussion. Many thanks are owed to Mr. J.-C. Jaud for the technical assistance in XRD analysis, to Mrs. K. Lakus-Wollny for the technical assistance in the morphological analysis and to Mrs. C. Fasel for the technical assistance in the thermal measurements. The author thanks the Federal Ministry of Research and Development (BMBF) (Project "*Perosol*" Nr. 03SF0483B) for the financial support during this work.

References

[1] S.D. Stranks and H.J. Snaith, Nature Nanotech. 10, (2015) 391-402.
[2] Z. Shi, J. Guo, Y. Chen, Q. Li, Y. Pan, H. Zhang, Y. Xia, W. Huang, Adv. Mater. 29 (2017) 1605005.
[3] T.M. Schmidt, T.T. Larsen-Olsen, J.E. Carle, D. Angmo and F.C. Krebs, Adv. En. Mater. 5 (2015), 1500569.
[4] L. Dimesso, M. Dimamay, M. Hamburger and W. Jaegermann, Chem. Mater. 26 (2014) 6762-6770.
[5] B. Hailegnaw, S. Kirmayer, E. Edri, G. Hodes and D. Cahen, J. Phys. Chem. Lett. 6 (2015) 1543–1547.
[6] Air Quality Standards, EU, http://ec.europa.eu/environment/air/quality/standards.htm,(accessed 15.06.2017).
[7] Scientific Commitee on Health and Environment Risks (SCHER), Report, 2011, © European Union, doi:10.2772/33674
[8] P. Patnaik, Handbook of Inorganic Chemicals, McGraw-Hill, New York 2003.
[9] K. Wang, Z. Liang, X. Wang and X. Cui, Adv. Electron. Mater. 1 (2015) 1500089.
[10] R.D. Shannon, Acta Crystallogr. A32 (1976) 751-767.
[11] P.G. Harrison, Chemistry of Tin, Ed.: Blackie, Glasgow (1989), Chapter 2, p. 9
[12] C.C. Stoumpos, C.D. Malliakas and M.G. Kanatzidis, Inorg. Chem. 52 (2013) 9019-9038.
[13] J. Yang, B.D. Siempelkamp, D. Liu and T.L. Kelly, ACS Nano 9 (2015) 1955–1963.
[14] N. Aristidou, I. Sanchez-Molina, T. Chotchuangchutchaval, M. Brown, L. Martinez, T. Rath and S. A. Haque, Angew. Chem. Int. Ed. 54 (2015) 8208–8212.
[15] B. Conings, J. Drijkoningen, N. Gauquelin, A. Babayigit, J. D'Haen, L. D'Olieslaeger, A. Ethirajan, J. Verbeeck, J. Manca, E. Mosconi, F. De Angelis and H.G. Boyen, Adv Energy Mater. 5 (2015) 1500477.
[16] L. Dimesso, C. Fasel, K. Lakus-Wollny, T. Mayer and W. Jaegermann, Mater. Sci. Semicond. Proc. 68 (2017) 152-158.
[17] A. Babayigit, D. Duy Thanh, A. Ethirajan, J. Manca, M. Muller, H.G. Boyen and B. Conings, Sci. Rep. 6 (2016) 18721.
[18] L. Dimesso, C. Das, T. Mayer and W. Jaegermann, J. Mater. Sci. (2018), in press, DOI: 10.1007/s10853-017-1545-0.
[19] D. Scaife, P. Weller and W. Fisher, J. Solid State Chem. 9 (1974) 308-314.
[20] L.S. Foster, H.G. Nahas and E.E. Lineken, Inorganic Syntheses, Volume 2, (ed. Fernelius WC), John Wiley & Sons, Inc., Hoboken, NJ, USA (1946).
[21] "Physical Constants of Inorganic Compounds," in CRC Handbook of Chemistry and Physics, 95th Edition (Internet Version 2015), W. M. Haynes, ed., CRC Press/Taylor and Francis, Boca Raton, FL.
[22] D.B. Mitzi, Chem. Mater. 8 (1996) 791-800.
[23] J. Andres, J. Krechl, M. Carda and E. Silla, Intern. J. Quantum Chem., Vol. XL (1991) 127-137.
[24] M.H. Almatarneh, C.G. Flinn and R.A. Poirier, Can. J. Chem. 83 (2005) 2082–2090.
[25] L. Dimesso, Y.M. Kim and W. Jaegermann, Mater. Sci. Engin. B 204 (2016) 27-33.
[26] T.M. Koh, T. Krishnamoorthy, N. Yantara, C. Shi, W.L. Leong, P.P. Boix, A.C. Grimsdale, S.G. Mhaisalkar and N. Mathews, J. Mater. Chem. A, 3 (2015) 14996–15000.
[27] R.L. Milot, G.E. Eperon, T. Green, H.J. Snaith, M.B. Johnston and L.M. Herz, J. Phys. Chem. Lett. 7 (2016) 4178–4184.

[28] X. Lü, Y. Wang, C.C. Stoumpos, Q. Hu, X. Guo, H. Chen, L. Yang, J.S. Smith, W. Yang, Y. Zhao, H. Xu, M.G. Kanatzidis and Q. Jia, Adv. Mater. 28 (2016) 8663-8668.

[29] A. Amat, E. Mosconi, E. Ronca, C. Quarti, P. Umari, M.K. Nazeeruddin, M. Graetzel and F. De Angelis, Nano Lett. 14 (2014) 3608–3616.

[30] L. Dimesso, C. Das, M. Stöhr and W. Jaegermann, Mater. Res. Bull. 85 (2017) 80-89.

[31] H.H. Fang, L. Protesescu, D.M. Balazs, S. Adjokatse, M.V. Kovalenko and M.A. Loi, Small (2017) 1700673 (DOI: 10.1002/smll.201700673).

[32] G. Gasparotto, S.A.M. Lima, M.R. Davolos, J.A. Varela, E. Longo and M.A. Zaghete, J. Luminescence 128 (2008) 1606–1610.

[33] Z. Liu, Q. Wang, Y. Yang, C. Tao and H. Yang, J. Nanopart. Res. 12 (2010) 2233–2240.

[34] R. Cao, W. Luo, H. Xu, Z. Luo, Q. Hua, T. Fu and D. Peng, Optical Materials 53 (2016)169–173.

[35] S.S. Novosad and R.O. Kovalyuk, Inorg. Mater. (Translation of Neorganicheskie Materialy) 33 (1997) 1183-1188.

[36] J. Chen, S. Wang, Y. Du and L. Chen, IEEE (2013) 978-1-4799-0534-8.

[37] P. Wang, J. Guan, D.T.K. Galeschuk, Y. Yao, C.F. He, S. Jiang, S. Zhang, Y. Liu, M. Jin, C. Jin and Y. Song, J. Phys. Chem. Lett. 8 (2017) 2119–2125.

Supporting Information

Enhanced thermal stability of formamidinium tin strontium iodide systems

The calculation of the theoretical weight % of Sn as component in the FASnI3 phase can be easily carried out as follows:
FASnI3: 1 mol = 544.49 g
Sn: 1 mol = 118.71 g
Sn (wt %) = (118.71 g / 544.49 g) * 100% = 21.80%
During the dynamic thermal analysis the overall decomposition of FASnI3 phase can occur as follows

$HC(NH_2)NH_2SnI_3$ (*s*) → HCN *(g)* + NH_3 (*g*) HI (*g*) + SnI_2 (*s*) (1)

SnI_2 (s) → SnI_2 (*liq*) (2)

SnI_2 (*liq*) → Sn (*s*) + SnI_4 (*g*) (3)

Assuming that:

(i) the reactions (1), (2) and (3) proceed to completion;

(ii) all gaseous products are taken away from the reaction site by the flowing carrier gas;

for the Law of conservation of mass we can reasonably suppose that at temperatures T ≥ 373°C, 1 mol of FASnI3 produces 1 mol of Sn(0). By observing Figure S1 we can suppose that the weight loss at T = 72°C can be attributed at volatile solvent residuals (black curve and scale), the remaining material consists of FASnI3 only. By considering FASnI3 as 100% wt of the analyzed material (red curve and scale in Figure S1), the wt% of the remaining material at T = 373°C (boiling point of SnI_4, reaction (3)) indicated with the green line in Figure S1 was 21.0% which is very close to the theoretical wt% value of Sn in the formamidinium containing perovskite. The obtained results would support the assumption of Sn(0) as residual material at T ≥ 373°C then the reactions (1)-(3).

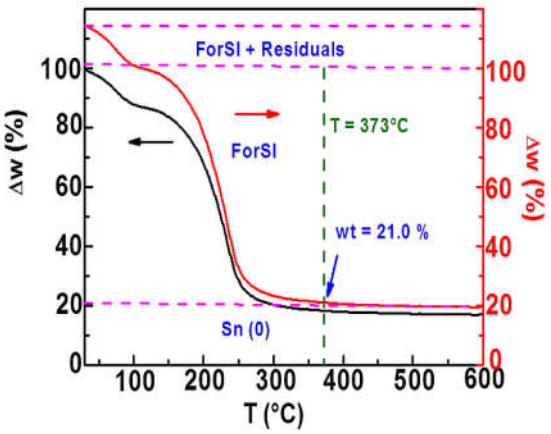

Figure S1. Measured TG profile (under flowing nitrogen, in black) and calculated TG profile (in red) for the ForSI system (x = 0.0).

(3)

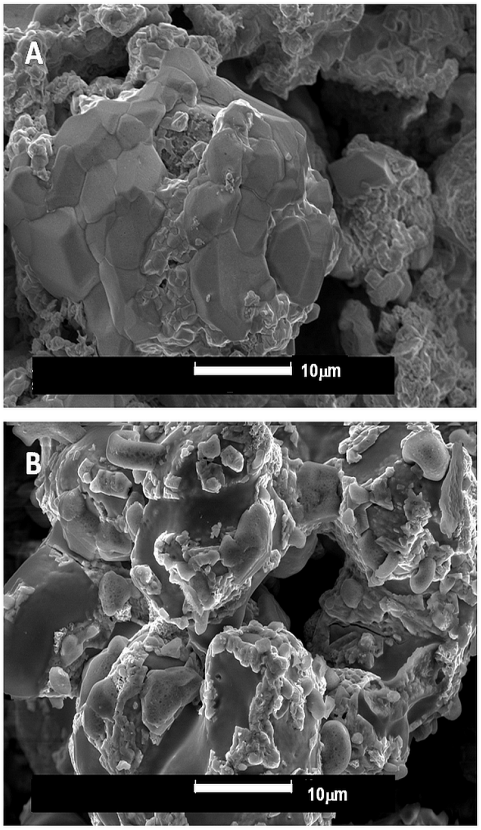

Figure S2. Typical SEM-images of $HC(NH_2)_2Sn_{1-x}Sr_xI_3$ systems annealed at T = 115°C for t = 8 hr under nitrogen for A) x = 0.0 and B) x = 0.05 respectively.

Table S1. Values of the fit parameters for the $HC(NH_2)_2Sn_{1-x}Sr_xI_3$ systems heated at T = 85°C and T = 150°C (t = 2h, under nitrogen) respectively, obtained from the data in Figure 5.

x	T(°C)	*a*	b_1	b_2	b_3	b_4	R^2
0.0							
	85[b)]	99.211±0.019	-0.027±0.002	$7.32x10^{-4}$±$7.53x10^{-5}$	-$9.80x10^{-6}$±9.38 $x10^{-7}$	$4.23x10^{-8}$±3.85 $x10^{-7}$	0.9674
	150[a)]	84.974±0.096	-0.183±0.001	-			0.9913
0.05	85[b)]	98.344±0.028	-0.019±0.003	$4.784x10^{-4}$±$1.22x10^{-4}$	-$7.92x10^{-6}$±$1.61x10^{-6}$	$3.90x10^{-8}$±$7.0x10^{-9}$	0.9692
	150[a)]	91.402±0.092	-0.206±0.001				0.9942
				-			
0.10	85	99.987±0.010	-	-	-		-
	150[a)]	89.739±0.006	0.219±$8.532x10^{-4}$	-			0.9977

[a)] A linear fit of the data was used: $y = a + b_1 \bullet x$

[b)] A polynomial fit of the data was used (n = 4): $y = a + b_1 \bullet x + b_2 \bullet x^2 + b_3 \bullet x^3 + b_4 \bullet x^4$